polymers

MDPI

Article

Synthesis, Property Characterization and Photocatalytic Activity of the Polyaniline/$BiYTi_2O_7$ Polymer Composite

Jingfei Luan *, Yue Shen, Shu Wang and Ningbin Guo

State Key Laboratory of Pollution Control and Resource Reuse, School of the Environment, Nanjing University, Nanjing 210093, China; yueshen_sally@outlook.com (Y.S.); wshgod@126.com (S.W.); MG1325044@smail.nju.edu.cn (N.G.)

* Correspondence: jfluan@nju.edu.cn; Tel.: +86-25-8968-0397; Fax: +86-25-8370-7304

Academic Editor: John T. Sheridan

Received: 13 December 2016; Accepted: 9 February 2017; Published: 23 February 2017

Abstract: A new polyaniline/$BiYTi_2O_7$ polymer composite was synthesized by chemical oxidation in-situ polymerization method for the first time. The effect of polyaniline doping on structural and catalytic properties of $BiYTi_2O_7$ was reported. The structural properties of novel polyaniline/$BiYTi_2O_7$ have been characterized by X-ray diffraction, scanning electron microscopy, X-ray photoelectron spectroscopy and UV-Vis DRS. The results showed that $BiYTi_2O_7$ crystallized well with the pyrochlore-type structure, stable cubic crystal system by space group Fd3m. The lattice parameter or band gap energy of $BiYTi_2O_7$ was found to be a = 10.2132 Å or 2.349 eV, respectively. The novel polyaniline/$BiYTi_2O_7$ polymer composite possessed higher catalytic activity compared with $BiYTi_2O_7$ or nitrogen doped TiO_2 for photocatalytic degradation of Azocarmine G under visible light irradiation. Additionally, the Azocarmine G removal efficiency was boosted from 3.0% for undoped $BiYTi_2O_7$ to 78.0% for the 10% polyaniline-modified $BiYTi_2O_7$, after only 60 min of reaction. After visible light irradiation for 330 min with polyaniline/$BiYTi_2O_7$ polymer composite as photocatalyst, complete removal and mineralization of Azocarmine G was observed. The photocatalytic degradation of Azocarmine G followed first-order reaction kinetics. Ultimately, the promoter action of H_2O_2 for photocatalytic degradation of AG with $BiYTi_2O_7$ as catalyst in the wastewater was discovered.

Keywords: polyaniline/$BiYTi_2O_7$; photocatalytic activity; Azocarmine G; visible light irradiation; H_2O_2

1. Introduction

The pollution of water resources by large quantities of azo-dyes effluents, generated from diverse industries such as chemical, textile or printing, due to their toxicity, high chemical oxygen demand content, and biological degradation, has a dramatically negative environmental impact, affecting the quality of drinking water. In the last decade, photocatalytic degradation processes had been widely applied as techniques for the destruction of organic pollutants in wastewater and effluents [1–20]. The photocatalytic degradation process has several advantages over other competing processes such as complete mineralization, no waste disposal problem, low cost, and only needing mild temperature and pressure [8].

Azocarmine G (AG) (Figure 1) as a common biological stain is often used to determine protein [21], DNA [22] and light neurons [23]. AG, a common kind of azo dye, is more difficult to handle. In exceptional circumstances, azo dyes can decompose to produce over 20 kinds of carcinogenic aromatic amines, which can cause lesions and induce cancer after activation to change the DNA

structure of the human body. Since the Sudan Red incident occurred, the use of biological stain and the wastewater treatment has been more cautious to the researchers. AG, however, is harder to be biodegraded and photodegraded directly. Many methods on the photodegradation of AG are reported. Unfortunately, most of these experiments were carried out under ultraviolet light irradiation. Nowadays, there are only a few reports for AG dye degradation under visible light irradiation, finding that the removal ratio of AG is very low.

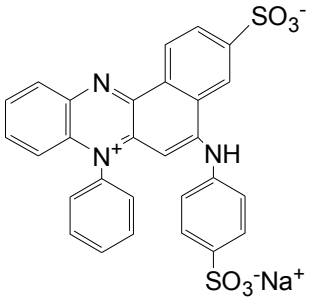

Figure 1. The molecular structure of Azocarmine G.

It is known that ultraviolet light only occupies 4% of the solar energy spectrum. For this reason, there is great interest in developing new visible light-responsive photocatalysts which are capable of utilizing the more ample visible light spectrum, which occupies about 43% of the solar energy range. Therefore, it is an urgent need to develop novel visible light-responsive photocatalysts. According to the past articles [24–29], many semiconductors can be used as photocatalysts under ultraviolet light irradiation, such as TiO_2 and ZnO.

In view of the efficient utilization of solar energy, numerous attempts have been made in recent years to develop different visible light-active photocatalysts [30–47]. Traditionally, for improving the photocatalytic efficiency of photocatalysts, the bandgap of photocatalysts or loaded cocatalysts plays an important role in photocatalyst system. Therefore, efficient catalysts that can generate electron–hole pairs under visible light irradiation should be developed [48–64]. Among them, $A_2B_2O_7$ compounds with narrow band gaps have been proven to be good candidates for photocatalytic degradation of organic pollutants under visible light irradiation. In our previous work [65], we found that In_2YbSbO_7 and Gd_2YbSbO_7 which owned the pyrochlore-type structure as a photocatalyst under visible light irradiation seemed to be potential for improvement of photocatalytic activity by modifying its structure.

A change and improvement of the electron transport and photophysical properties could be found in the novel $BiYTi_2O_7$ compound which might display advanced photocatalytic properties. $BiYTi_2O_7$ had never been produced and the data about its structural such as space group and lattice constants had not been previously reported. In addition, the photocatalytic properties of $BiYTi_2O_7$ had not been investigated by other investigators. The molecular composition of $BiYTi_2O_7$ was very similar to that of other $A_2B_2O_7$ compounds. $BiYTi_2O_7$ also seemed to have potential for improvement of photocatalytic activity by modifying its structure, because it had been proven that a slight modification of a semiconductor structure would cause a remarkable change in photocatalytic properties.

Polyaniline (PANI) has a high application rate in view of its electrical and optical properties, ease of derivatization, solubility in several solvents, processability inside fibers and films, and stability [66–68]. In addition, PANI with delocalized π-conjugated structures is beneficial to rapid charge separation, thus the separation efficiency of photogenerated electron (e^-)–hole (h^+) pairs can be significantly improved [69]. Shang et al. [70] reported that on the basis of the small grain size, the intrinsic property of PANI, and the synergic effect between PANI and $BiVO_4$, a rapid electron–hole separation and slow recombination was realized. Hidalgo et al. [71] prepared PANI–TiO_2 nanocomposites by a novel and green sol-gel spin coating method. The results showed that the photocurrent in PANI/TiO_2 electrodes dramatically increased under simulated sunlight irradiation, reaching maximum photocurrent densities around 2 and 1.6 fold higher than the pristine TiO_2 NPs.

Moreover, due to the excellent environmental stability of polyaniline, the polyaniline–hybridized $BiYTi_2O_7$ sample should possess more advanced photocatalytic properties. Thus, the resemblance suggested that $BiYTi_2O_7$ and the polyaniline–hybridized $BiYTi_2O_7$ may own photocatalytic properties under visible light irradiation, like other members in the $A_2B_2O_7$ family.

For the purpose of further designing novel high–efficiency and stable photocatalysts, in this study, polyaniline with ultra-low loading amount (1%, 5% and 10%) was loaded onto $BiYTi_2O_7$ to synthesize polyaniline/$BiYTi_2O_7$ polymer composites by the chemical oxidation polymerization method for the first time. The structural and photocatalytic properties of the polyaniline–hybridized $BiYTi_2O_7$ were studied in detail. The photocatalytic property was evaluated by the degradation of AG under visible light irradiation. The 10% polyaniline–hybridized $BiYTi_2O_7$ exhibited excellent photocatalytic activity. In order to elucidate the structure–photocatalytic activity relationship in the polyaniline–hybridized $BiYTi_2O_7$, a comparison among the photocatalytic properties of the polyaniline–hybridized $BiYTi_2O_7$, $BiYTi_2O_7$ and nitrogen doped TiO_2 (N-doped TiO_2) was carried out. The reaction mechanism of the improved photocatalytic performance of polyaniline/$BiYTi_2O_7$ polymer composites was also investigated.

2. Materials and Methods

2.1. Preparation Method of $BiYTi_2O_7$

The novel photocatalyst had been synthesized by solid-state reaction method. Bi_2O_3, Y_2O_3, and TiO_2 with purity of 99.99% (Sinopharm Group Chemical Reagent Co., Ltd., Shanghai, China) were used as starting materials without further purification. Owing to the volatility of Bi_2O_3, the molar ratio of atoms in $BiYTi_2O_7$ (n(Bi):n(Y):n(Ti):n(O)) does not close to the stoichiometric ratio of 1:1:2:7 after the experiment, therefore, we finally decided to add 130% quantities of Bi_2O_3 after 5 experiments to gain pure $BiYTi_2O_7$ catalyst. All powders (n(Bi_2O_3):n(Y_2O_3):n(TiO_2) = 1.3:1:4) were dried at 200 °C for 4 h before synthesis. In order to synthesize $BiYTi_2O_7$, the precursors were stoichiometrically mixed, then pressed into small columns and put into an alumina crucible (Shenyang Crucible Co., Ltd., Shenyang, China). After the raw materials calcining at 400 °C for 2 h, then at 750 °C for 10 h, we took the small columns out of the electric furnace, ground the mixed materials and subsequently put them into the electric furnace (KSL 1700X, Hefei Kejing Materials Technology Co., Ltd., Hefei, China). The mixed materials were calcined at 1050 °C for 30 h with an intermediate regrinding process in an electric furnace. Finally, pure $BiYTi_2O_7$ catalyst, which presented the color of light yellow, was obtained after total grinding. One hundred-gram samples were synthesized at a time.

2.2. Preparation of Polyaniline–Hybridized $BiYTi_2O_7$

An amount of distilled aniline (0.2, 1 or 2 g) was added to 150 mL of 1M HCl, and subsequently stirred for 30 min to ensure that the aniline was totally dissolved. Subsequently, a certain percentage of $BiYTi_2O_7$ (19.8, 19 or 18 g, respectively) was added into above solution, sonicated for 30 min to obtain a dispersed solution, and then stirred for 1 h. Thirdly, 0.5 g·mL^{-1} ammonium thiosulfate (HCl) was added into the solution slowly; subsequently, the mixture was stirred for 24 h with the final color of deep green. Finally, the suspension was filtered, and the precipitate was washed with alcohol and water for many times and dried at 60 °C to obtain polyaniline (PANI)–hybridized-$BiYTi_2O_7$. In this article, we named the photocatalysts which were m(PANI):m($BiYTi_2O_7$) = 1:100, 5:100, and 10:100 as $BiYTi_2O_7$-1%PANI, $BiYTi_2O_7$-5%PANI, and $BiYTi_2O_7$-10%PANI, respectively. The batch size among three synthesized samples was 20 g at a time.

2.3. Characterization of $BiYTi_2O_7$ and PANI–$BiYTi_2O_7$

The crystal structures of $BiYTi_2O_7$ and PANI–$BiYTi_2O_7$, were analyzed by the powder X-ray diffraction method (D/MAX-RB, Rigaku Corporation, Tokyo, Japan) with Cu$K\alpha$ radiation (λ = 1.54056). The data were collected at 295 K with a step-scan procedure in the range of 2θ = 10°–100°. The step

interval was 0.02° and the time per step was 1.2 s. The chemical composition of the compound was determined by Scanning Electron Microscope-X-ray Energy Dispersion Spectrum (SEM-EDS, LEO 1530VP, LEO Corporation, Dresden, Germany). The Bi^{3+} content, Y^{3+} content, Ti^{4+} content, and O^{2-} content of $BiYTi_2O_7$ were determined by X-ray photoelectron spectroscopy (XPS, ESCALABMK-2, VG Scientific Ltd., London, UK). The chemical composition within the depth profile of $BiYTi_2O_7$ was examined by the argon ion denudation method when X-ray photoelectron spectroscopy was used. The optical absorption of $BiYTi_2O_7$ and PANI–$BiYTi_2O_7$ was analyzed with an UV-Visible spectrophotometer (UV-2450, Shimadzu Corporation, Kyoto, Japan). The particle sizes of the photocatalysts were determined by Malvern's Mastersize-2000 particle size analyzer (Malvern Instruments Ltd., Malvern, UK).

2.4. Photocatalytic Characterizations of $BiYTi_2O_7$ and PANI–$BiYTi_2O_7$

The photocatalytic degradation experiments of AG were carried out with photocatalyst powders which were suspended in 50 mL 20 mg·L^{-1} solution in 12 identical Pyrex glass cells (Nanjing Xujiang Industry, Nanjing, China). Before light irradiation, the suspensions were magnetically stirred in the darkness for 30 min to ensure establishment of an adsorption-desorption equilibrium among photocatalyst, the dye and atmospheric oxygen. The photocatalytic reaction system consisted of a 500 W Xe arc lamp (Nanjing Xujiang Industry, Nanjing, China), a magnetic stirrer and a cut-off filter ($\lambda > 420$ nm, Nanjing Xujiang Industry, Nanjing, China). The Xe arc lamp was surrounded by a quartz jacket and was positioned in a photoreactor quartz vessel. Room temperature (25 °C) was maintained by an outer recycling water glass jacket. The solution was continuously stirred magnetically. After every 30 min, one of the Pyrex glass cells was sampled. Without pH adjustment, the initial pH value was 6.0 for AG. Additionally, the concentration of AG was determined according to the absorption wavelength at 524 nm as measured by a UV-Vis spectrophotometer (UV-2550, Shimadzu Corporation, Kyoto, Japan), since the highest absorption wavelength of AG was 524 nm. The total organic carbon (TOC) concentration was determined with a TOC analyzer (TOC-5000, Shimadzu Corporation).

3. Results and Discussion

3.1. Characterization

3.1.1. XRD Analysis

The structure with full-profile refinements of the as-prepared product $BiYTi_2O_7$ was examined by X-ray diffraction technique and the results were shown in Figure 2. The collected data was obtained by the Materials Studio program, which was based on Rietveld analysis. The powder X-ray diffraction analysis revealed that the product could be melted when sintering temperature was over 1150 °C. In the light of Figure 2, it could be concluded that $BiYTi_2O_7$ was single phase and that the lattice parameter for this new photocatalyst $BiYTi_2O_7$ was 10.21323 Å. Simultaneously, the final refinement for $BiYTi_2O_7$ showed a good agreement between the observed and calculated intensities for the pyrochlore-type structure, a cubic crystal system and a space group Fd3m (O atoms are included in the model). In addition, all of the diffraction peaks for this photocatalyst could be indexed successfully, according to the lattice constant and above space group. Moreover, the atomic coordinates and structural parameters of $BiYTi_2O_7$ are recorded in Table 1.

As can be seen from the X-ray diffraction, it could be concluded that $BiYTi_2O_7$ crystallized into pyrochlore-type structure. The cubic system structure with space group Fd3m for $Bi_2Ti_2O_7$ keeped unchanged after Bi^{3+} being substituted by Y^{3+}. The results of full-profile structure refinements for $BiYTi_2O_7$ generated the unweighted *R* factors, R_P = 13.80% with space group Fd3m. Contrary to the work of Zou et al. [72], Bi_2InNbO_7 which was slightly modified had a larger *R* factor.

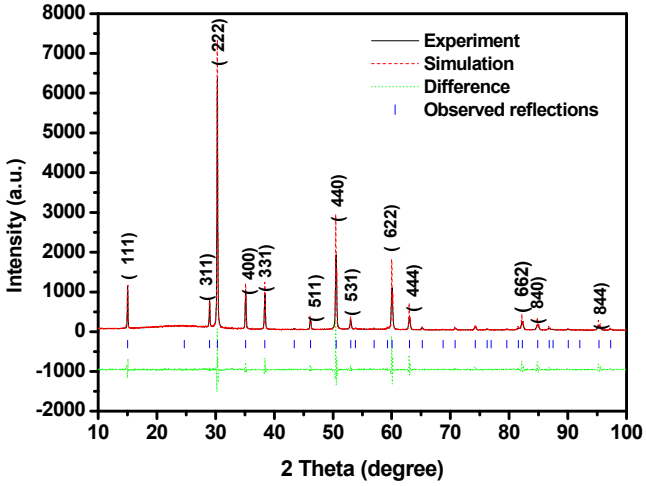

Figure 2. X-ray powder diffraction patterns and Rietveld refinements of $BiYTi_2O_7$ (black solid line represents experimental XRD data; red dotted line represents simulative XRD data; green dashed line represents a difference between experimental XRD data and simulative XRD data; and blue vertical line represents observed reflection positions).

Table 1. Structural parameters of $BiYTi_2O_7$ prepared by solid state reaction method.

Atom	*x*	*y*	*z*	Occupation factor
Bi	0.5	0.5	0.5	0.5
Y	0.5	0.5	0.5	0.5
Ti	0	0	0	1
O(1)	0.375	0.375	0.375	1
O(2)	0.125	0.125	0.125	1

Figure 3 presents the XRD pattern of different polyaniline based on $BiYTi_2O_7$. As shown in Figure 3, all the diffraction peaks of different polyaniline loaded on $BiYTi_2O_7$ were absolutely similar to $BiYTi_2O_7$ with pyrochlore-type structure. It could reveal that the structures of different polyaniline based on $BiYTi_2O_7$ were determined by the cubic structure of $BiYTi_2O_7$. The addition of polyaniline would not change the lattice structure of $BiYTi_2O_7$. In addition, the polyaniline parcel layer was very thin because we could not detect the diffraction peaks of polyaniline [73].

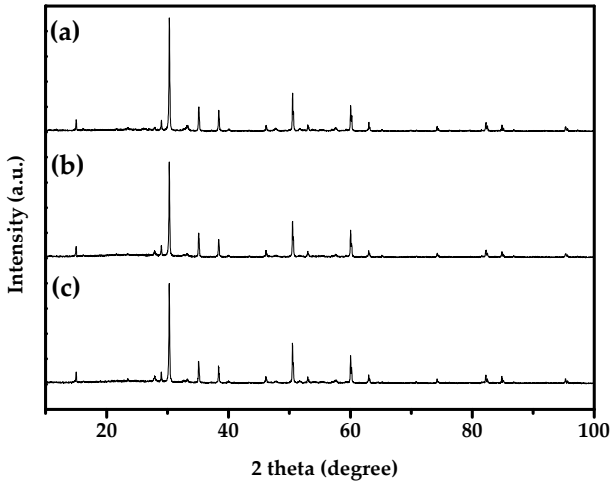

Figure 3. X-ray diffraction patterns of: (**a**) $BiYTi_2O_7$-1%PANI; (**b**) $BiYTi_2O_7$-5%PANI; and (**c**) $BiYTi_2O_7$-10%PANI.

3.1.2. SEM Analysis

The SEM image of $BiYTi_2O_7$ (Figure 4) shows that the $BiYTi_2O_7$ particle size is relatively uniform. The SEM-EDS spectrum of $BiYTi_2O_7$ (Figure 5) revealed that $BiYTi_2O_7$ was pure phase without any other impurities but bismuth, yttrium, titanium and oxygen (where the C peak was introduced by the necessary conductive paste in the energy spectrum analysis). Moreover, the molar ratio of its atoms (n(Bi):n(Y):n(Ti):n(O)) closed to the stoichiometric ratio of 1:1:2:7. It was impossible that the space groups we observed were generated from impurities. Therefore, it could conclude that the slight R factor of this photocatalyst was resulted from slightly modified structure model. Furthermore, the change of structures, including different bond-distance distributions, thermal displacement parameters and/or occupation factors for some of the atoms, were due to the defects or the disorder/order of a part of the atoms [74].

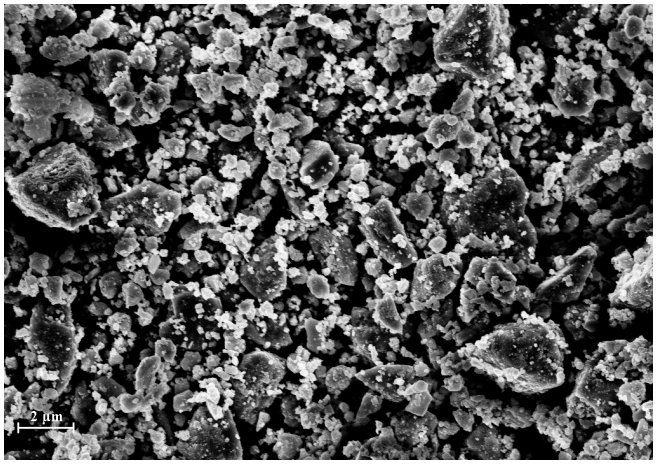

Figure 4. SEM spectra of $BiYTi_2O_7$.

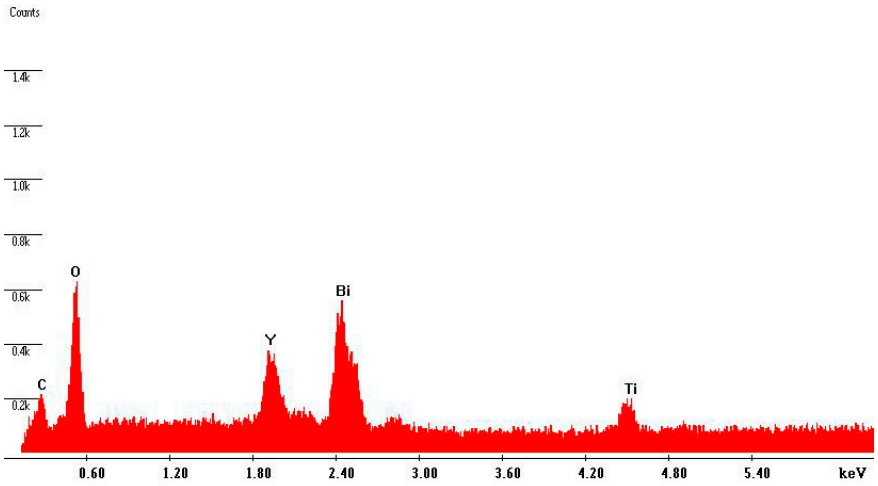

Figure 5. EDS spectra of $BiYTi_2O_7$.

The SEM images of different polyaniline based on $BiYTi_2O_7$ (Figure 6) presented that, with the increase in the amount of polyaniline doped on the surface of $BiYTi_2O_7$ particle, the composite photocatalyst turned into coarser and coarser gradually. The layered material on the surface of $BiYTi_2O_7$ particle was polyaniline, adsorped on $BiYTi_2O_7$ particles by physical adsorption. Moreover, the SEM-EDS spectrum of different polyaniline based on $BiYTi_2O_7$ also revealed that the photocatalysts were pure phase without any other impurities but bismuth, yttrium, titanium, carbon, nitrogen and oxygen.

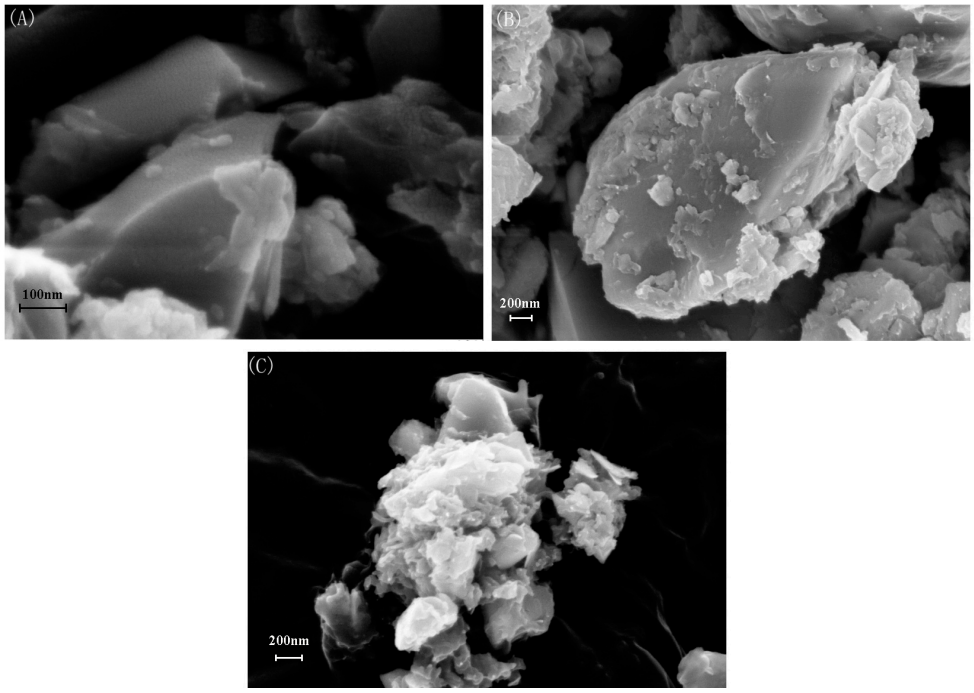

Figure 6. SEM images of: (**A**) $BiYTi_2O_7$-1%PANI; (**B**) $BiYTi_2O_7$-5%PANI; and (**C**) $BiYTi_2O_7$-10%PANI.

3.1.3. XPS Analysis

To further determine the chemical composition of the photocatalyst $BiYTi_2O_7$, X-ray photoelectron spectroscopy (XPS) measurement was carried out. The XPS survey scan spectra of $BiYTi_2O_7$ was supplied in Figure 7. Various elemental peaks, which correspond to specific binding energies of $BiYTi_2O_7$, are provided in Table 2. The binding energies of $Bi4f_{5/2}$, $Bi4f_{7/2}$, $Y3d_{3/2}$, $Y3d_{5/2}$, $Ti2p_{1/2}$ and $Ti2p_{3/2}$ in $BiYTi_2O_7$ were 163.3, 156.5, 157.9, 158.6, 463.8 and 457.2 eV, respectively. The binding energies of $Bi4f_{7/2}$ in $BiYTi_2O_7$ after carbon revision was 157.2 eV, compared with that in experimentation, revealing that the characteristic peak of $Bi4f_{7/2}$ shifted to the lower energy. The main reason might be that the replacement of a part of Bi (2.02 for electronegativity) by Y (1.22 for electronegativity) resulted in a decrease in the electronegativity of the atoms around the Bi [75].

The consequence represented that the oxidation state of Bi, Y, Ti and O ions from $BiYTi_2O_7$ were +3, +3, +4 and −2, respectively. In addition, the average atomic ratio of Bi:Y:Ti:O for $BiYTi_2O_7$ was calculated to be the same as 1:1:2:7, based on our XPS and SEM-EDS. Consequently, it could be deduced that under our preparation condition, the resulting material was highly pure. As can be seen in Table 2, it could be found that there were two peaks with different binding energies for oxygen (O1s). The split of O1s peaks in Figure 7c was assigned to O1s peaks of crystal lattice oxygen (528.8 eV) and surface adsorbed oxygen (530.4 eV) [76]. Figure 7c shows that the XPS peak of O1s was asymmetrical, and there was acromion in the direction of higher binding energy (>530.1 eV). We fitted the O1s XPS peak, and it concluded that the Peak C1 was surface lattice oxygen species of photocatalyst, and that the Peak C2 was adsorbed oxygen on the catalyst surface after the calcination process.

Table 2. Binding energies of key elements in $BiYTi_2O_7$.

$BiYTi_2O_7$	Bi4f		Y3d		Ti2p		O1s	C1s
	$Bi4f_{5/2}$	$Bi4f_{7/2}$	$Y3d_{3/2}$	$Y3d_{5/2}$	$Ti2p_{1/2}$	$Ti2p_{3/2}$		
Experimental (eV)	163.3	156.5	157.9	158.6	463.8	457.2	528.8	283.9
After carbon revision (eV)	164.0	157.2	158.6	159.3	464.5	457.2	529.5	284.8

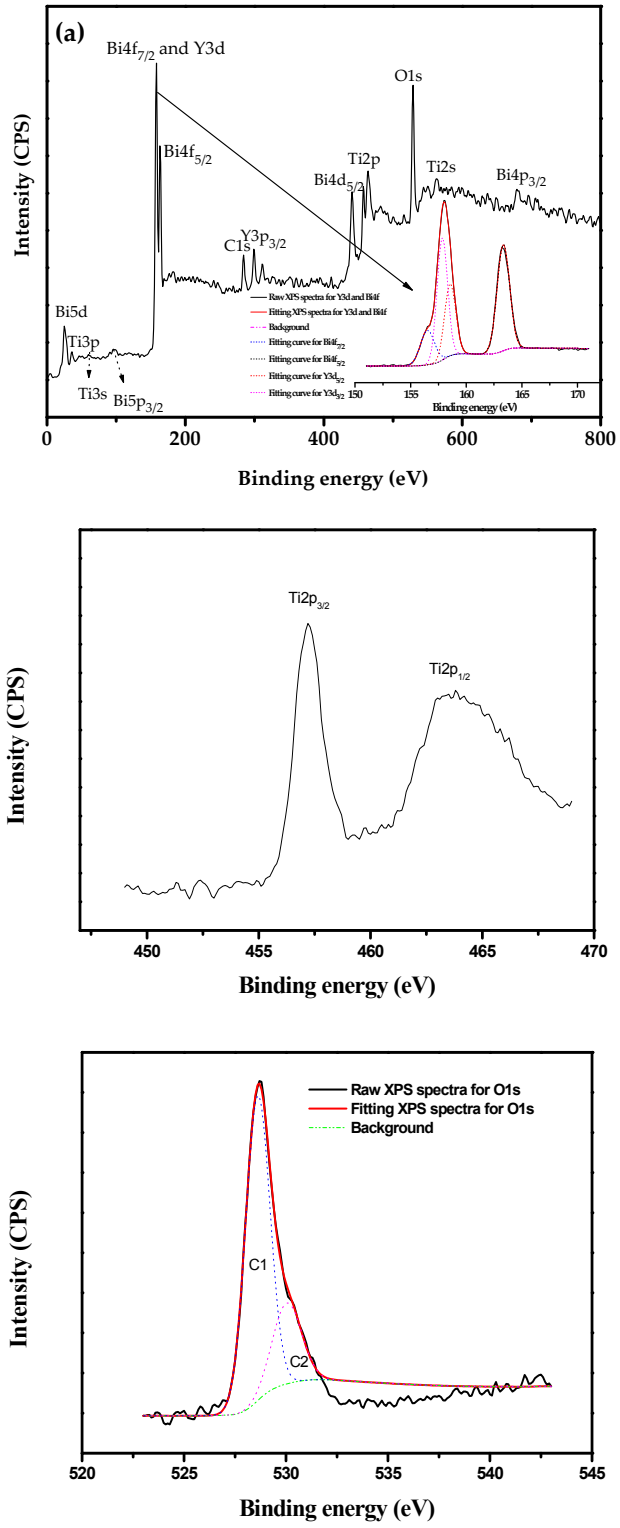

Figure 7. (**a**) Full XPS regions for $BiYTi_2O_7$ (Inset is the enlarged range of the Bi4f and Y3d peak); XPS spectra of: (**b**) Ti2p; and (**c**) O1s of $BiYTi_2O_7$.

3.1.4. UV-Vis Diffuse Reflectance Spectra

The absorption spectra of $BiYTi_2O_7$, $BiYTi_2O_7$-1%PANI composite and N-doped TiO_2 samples are listed in Figure 8. Compared with well-known N-doped TiO_2 whose absorption edge was no more than 420 nm, the absorption edge of this new photocatalyst was found to be at 527 nm for $BiYTi_2O_7$,

i.e., at the visible region of the spectrum. Meanwhile, compared with $BiYTi_2O_7$, $BiYTi_2O_7$-1%PANI photocatalyst increased in the entire absorption spectral range.

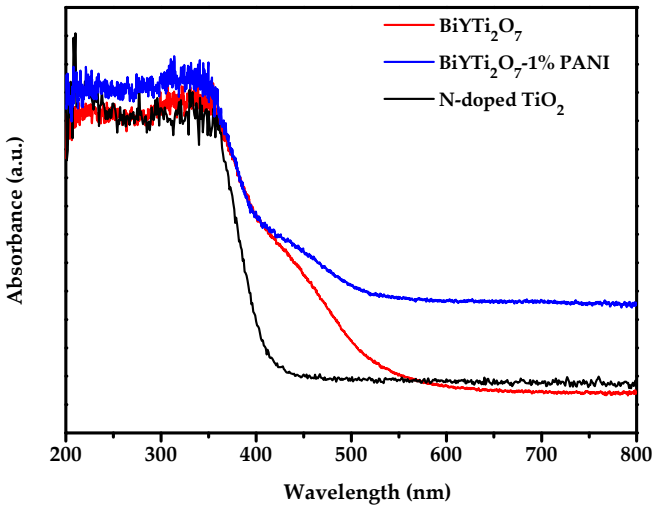

Figure 8. Absorption spectra of $BiYTi_2O_7$, $BiYTi_2O_7$-1% PANI and N-doped TiO_2.

We realized that absorbance could not be proportional to one-transmission, thus the absorbance was calculated using the Kubelka–Munk transformation method in our experiment. The optical absorption near the band edge of the crystalline semiconductors obeys the equation [77,78]:

$$\alpha h\nu = \mathrm{A}\ (h\nu - E_g)^n \quad (1)$$

where A, α, E_g and ν represent proportional constant, absorption coefficient, band gap and light frequency, respectively. Within this equation, n determines the character of the transition in a semiconductor. E_g and n can be calculated by the following steps: (1) plotting $\ln(\alpha h\nu)$ versus $\ln(h\nu - E_g)$ assuming an approximate value of E_g; (2) deducing the value of n based on the slope in this graph; and (3) refining the value of E_g by plotting $(\alpha h\nu)^{1/n}$ versus $h\nu$ and extrapolating the plot to $(\alpha h\nu)^{1/n} = 0$. According to the above method, the values of E_g for $BiYTi_2O_7$, $BiYTi_2O_7$-1%PANI and N-doped TiO_2 were calculated to be 2.349, 2.476 and 2.952 eV, respectively. The estimated value of n was about 0.5 and the optical transition for these photocatalysts was allowed directly. The results showed that $BiYTi_2O_7$-1%PANI possessed a little wider band gap compared with $BiYTi_2O_7$. However, on account of the rapid charge separation from PANI with delocalized π-conjugated structures, $BiYTi_2O_7$-1%PANI could produce more electron–hole pairs and lead to higher photocatalytic activity under visible light.

3.1.5. Band Structures

Figure 9 presents the advisable band structures of $BiYTi_2O_7$. Recently, Oshikiri et al. [79] reported that the electronic structures of $InMO_4$ (M = V, Nb and Ta) and $BiVO_4$ were described based on first principles calculations. The conduction bands of the $InMO_4$ (M = V, Nb and Ta) as photocatalysts were mainly composed of a dominant d orbital component from V 3*d*, Nb 4*d* and Ta 5*d* orbitals. Meanwhile, the valence bands of the $BiVO_4$ as photocatalysts were composed of a minor Bi 6*s* orbital component and a dominant O 2p orbital component. Similarly, the band structures of $BiYTi_2O_7$ should be similar to $InMO_4$ (M = V, Nb and Ta) and $BiVO_4$. Therefore, we deduced that, in the $BiYTi_2O_7$, the conduction band was composed of Y 4*d* and Ti 3*d* orbital component, and the valence band was composed of a small Bi 6s and O 2p orbital component. $BiYTi_2O_7$ could produce electron–hole pairs by absorption of photons directly, indicating that the enough energy which was larger than that between the conduction and valence band was necessary for decomposing AG photocatalysis process.

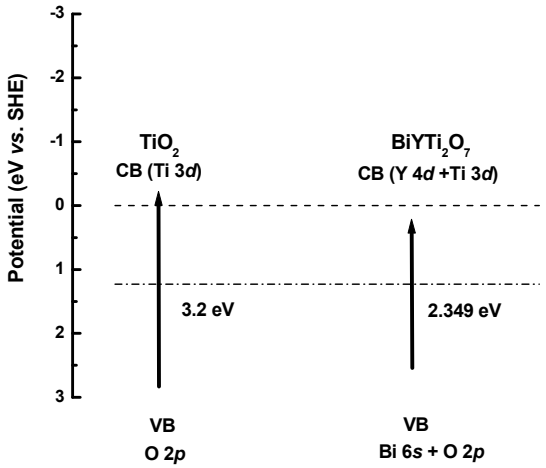

Figure 9. Suggested band structures of $BiYTi_2O_7$.

3.2. Photocatalytic Properties of Different PANI-Modified $BiYTi_2O_7$ Photocatalysts

Figure 10 shows UV-Vis absorption spectra of different concentrations of AG. The results showed a reduction in the typical AG peaks at 524 nm. The absorbency standard curve of AG was illustrated in Figure 11. Subsequently, the standard curve equation of AG was $A = 0.0215\ C - 0.0003$. Here, A and C, respectively, represent proportional constant and the concentrations of AG. Therefore, according to the standard curve equation of AG, the removal rate of AG was $D\% = (C_0 - C_t)/C_0 \times 100\%$.

Figure 12 shows the chart for the adsorption of AG by $BiYTi_2O_7$ in the absence of visible light and photolysis of AG without any photocatalyst. As depicted in Figure 12, the suspension had already reached adsorption/desorption equilibrium between the dye and the catalyst when stirred in the dark for 30 min. Moreover, even in the absence of a photocatalyst, the concentration of AG decreased lightly under visible light irradiation. As a result, the rate of AG degradation was estimated to be 0.22366×10^{-9} mol·L^{-1}·s^{-1} after visible light irradiation within 360 min. It could be illustrated that the decrease on the concentration of dye without any photocatalyst was ascribed to the direct dye sensitization effect, which was similar to the observation from Liu et al. [80]. On the other side, the possible reason of slightly promoting photocatalytic effect was that $BiYTi_2O_7$ had a absorption effect for little dye without visible light irradiation. Generally, the direct absorption of band-gap photons and the generation of electron–hole pairs in the semiconductor particles leaded the photocatalytic activity [81]. Then, the charge carriers began to diffuse to the surface of the particle. Consequently, the photocatalytic activity for decomposing organic compounds with these semiconductor catalysts was enhanced.

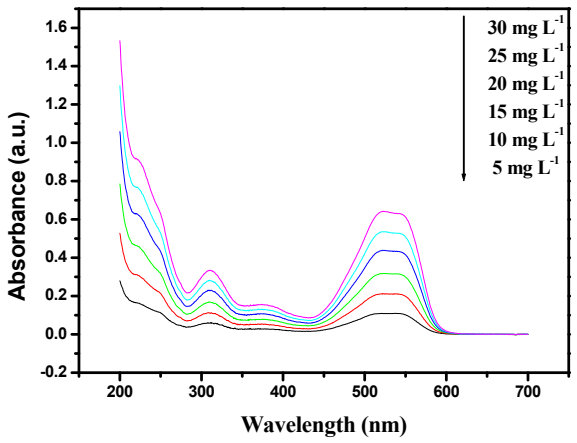

Figure 10. UV-Vis absorption spectra of different concentrations of AG.

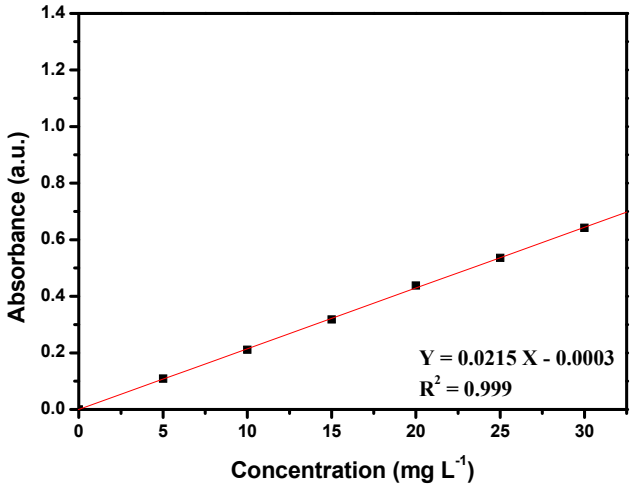

Figure 11. Absorbency standard curve of AG.

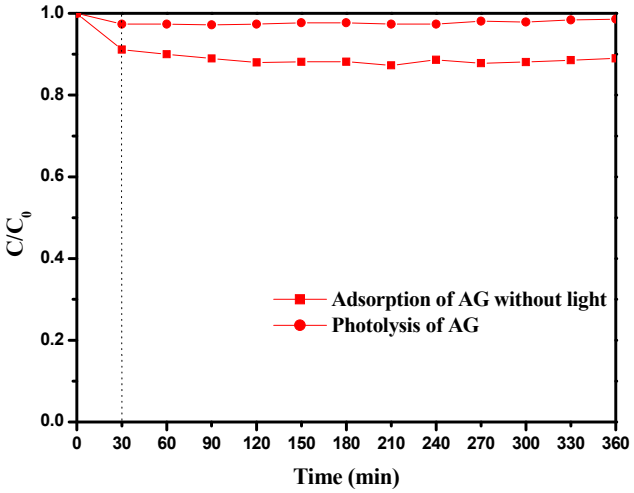

Figure 12. Adsorption and photolysis for AG dye.

Figure 13 is the chart for removal rate of AG (50 mL 20 mg·L^{-1}) with 2 g·L^{-1} different PANI-modified $BiYTi_2O_7$ photocatalysts under visible light. The results showed that the removal rate of AG is only 18.0% or 16.1% using $BiYTi_2O_7$ or N-doped TiO_2 as catalyst under visible light irradiation within 330 min. Similarly, the removal rate of AG was about 29.9%, 69.6% and 100%, respectively, when the $BiYTi_2O_7$-1%PANI, $BiYTi_2O_7$-5%PANI and $BiYTi_2O_7$-10%PANI were used as photocatalysts under visible light irradiation within 330 min. Additionally, the AG removal efficiency was boosted from 3.0% for undoped $BiYTi_2O_7$ to 78.0% for the 10% PANI-modified $BiYTi_2O_7$, after only 60 min of reaction. It could be concluded that the photocatalytic effects were enhanced with the improvement of polyaniline content loaded on the photocatalysts. AG was converted to small organic species and mineralized into inorganic products (CO_2 and water) by photogenerated electrons and holes from different PANI-modified $BiYTi_2O_7$. To sum up, the photocatalytic degradation activity of these new photocatalysts was faster than common photocatalyst N-doped TiO_2 which had a little effect on photodegrading AG under visible light. The main reason was that N-doped TiO_2 had little response in the visible region, and the removal of AG with N-doped TiO_2 was coming from the effects of absorption and photolysis.

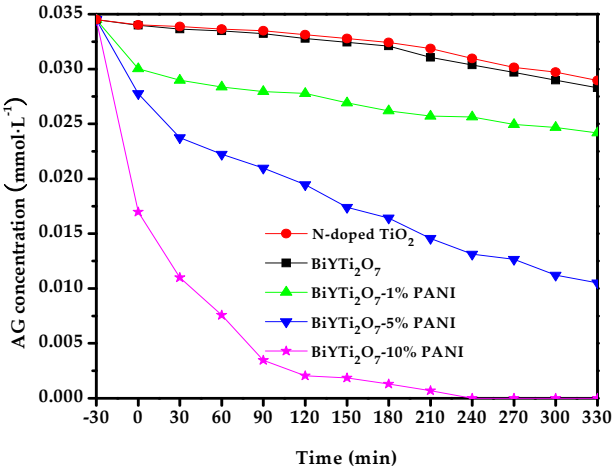

Figure 13. Photocatalytic degradation of AG under visible light irradiation in the presence of different PANI-modified $BiYTi_2O_7$ photocatalysts and N-doped TiO_2.

Figure 14 presents the change of TOC for the photocatalytic degradation of AG (50 mL 20 mg·L^{-1}) during visible light irradiation with 2 g·L^{-1} different PANI-modified $BiYTi_2O_7$ or N-doped TiO_2 as a photocatalyst, which is in accordance with the tendency shown in Figure 13. The gradual decrease of TOC represented the gradual disappearance of organic carbon when the AG solution which contained different PANI-modified $BiYTi_2O_7$ or N-doped TiO_2 was exposed under visible light irradiation. The removal rate of TOC was 15.90%, 28.93%, 65.38%, 100% and 13.87% with $BiYTi_2O_7$, $BiYTi_2O_7$-1%PANI, $BiYTi_2O_7$-5%PANI, $BiYTi_2O_7$-10%PANI and N-doped TiO_2 as a catalyst, respectively, after visible light irradiation for 330 min. Moreover, the reactions stopped when the light was turned off in this experiment, which showed the obvious light response, suggesting that AG had been converted to other kinds of byproducts and the organic carbon in the AG had not been decomposed to CO_2 [82].

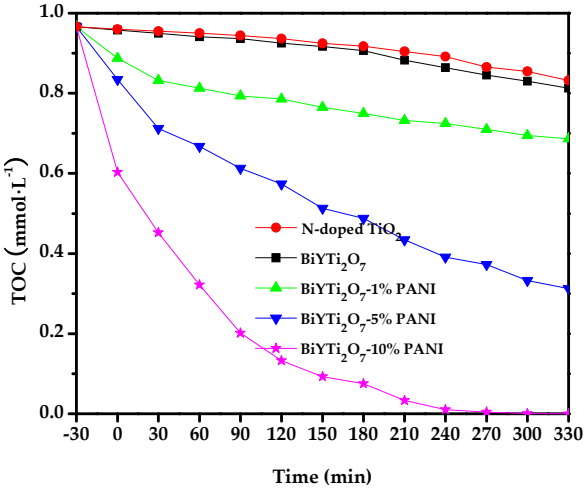

Figure 14. Disappearance of the total organic carbon (TOC) during the photocatalytic degradation of AG with different PANI-modified $BiYTi_2O_7$ and N-doped TiO_2 as a catalyst under visible light irradiation.

Figure 15 shows the amount of variation of CO_2 produced during the photocatalytic degradation of AG (50 mL 20 mg·L^{-1}) using 2 g·L^{-1} different PANI-modified $BiYTi_2O_7$ or N-doped TiO_2 as a photocatalyst under visible light irradiation. After visible light irradiation of 330 min, the CO_2

production of 0.09105, 0.16552, 0.39032 and 0.57958 mmol with $BiYTi_2O_7$, $BiYTi_2O_7$-1%PANI, $BiYTi_2O_7$-5%PANI and $BiYTi_2O_7$-10%PANI as a catalyst, respectively, was higher than that of 0.07925 mmol with N-doped TiO_2. In addition, the amount of CO_2 production was nearly equivalent to that of the removed TOC. At the same time, the amount of CO_2 production or that of the removed TOC was slightly lower than that of reduced AG by using different photocatalysts relative to the C element equilibrium, indicating that AG was mainly degraded into some inorganic products including CO_2 and eventually H_2O.

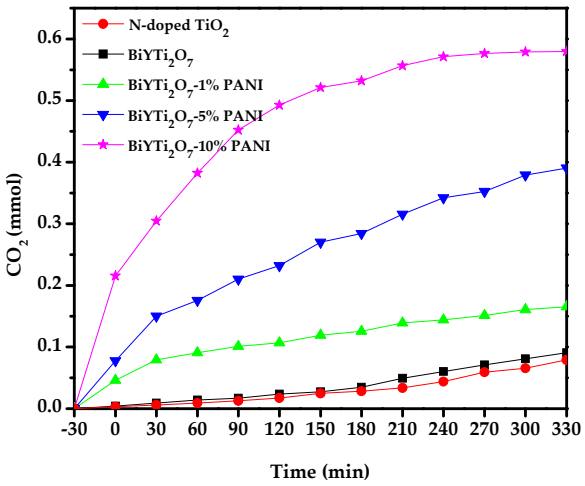

Figure 15. CO_2 production kinetics during the photocatalytic degradation of AG with different PANI-modified $BiYTi_2O_7$ and N-doped TiO_2 as a catalyst under visible light irradiation.

There was a linear correlation between $\ln(C/C_o)$ and the irradiation time for the (visible light) photocatalytic AG degradation with the presence of these novel photocatalysts. Here, C represented the AG concentration at time t, and C_o represented the initial AG concentration. According to Table 3, the first-order rate constant k of AG concentration with $BiYTi_2O_7$, $BiYTi_2O_7$-1%PANI, $BiYTi_2O_7$-5%PANI and $BiYTi_2O_7$-10%PANI were estimated. In addition, the different values of k indicated that PANI-modified $BiYTi_2O_7$ photocatalysts were more suitable for the photocatalytic degradation of AG under visible light irradiation than $BiYTi_2O_7$ photocatalyst.

Table 3. Kinetics parameters of photocatalytic degradation of AG with $BiYTi_2O_7$, $BiYTi_2O_7$-1%PANI, $BiYTi_2O_7$-5%PANI and $BiYTi_2O_7$-10%PANI.

Photocatalysts	R	Regression equation	K (h^{-1})
$BiYTi_2O_7$	0.9697	$Y = 0.0337X - 0.0052$	0.0337
$BiYTi_2O_7$-1%PANI	0.9877	$Y = 0.0379X + 0.1515$	0.0379
$BiYTi_2O_7$-5%PANI	0.9648	$Y = 0.2441X + 0.1698$	0.2441
$BiYTi_2O_7$-10%PANI	0.9874	$Y = 0.9004X + 0.7508$	0.9004

In order to study the stability of performance for PANI-modified $BiYTi_2O_7$ as a visible light catalyst, repeated photocatalytic degradation tests of AG with 10% PANI-modified $BiYTi_2O_7$ as photocatalyst under visible light irradiation was carried out. As can be seen in Figure 16, the removal efficiencies of AG were 98.2%, 96.0% and 92.5% for the second, third and fourth cycles, respectively, after visible light irradiation of 330 min. Figure 16 indicates that the activity slightly decreased after the first cycle, which was probably due to a small drop of 7.5% in the amount of 10% PANI modified $BiYTi_2O_7$ particles. Although the photocatalytic degradation efficiency of AG dropped from 100% for the first cycle to 92.5% for the fourth cycle, 10% PANI-modified $BiYTi_2O_7$ still showed excellent stability and was considered to be an efficient photocatalyst.

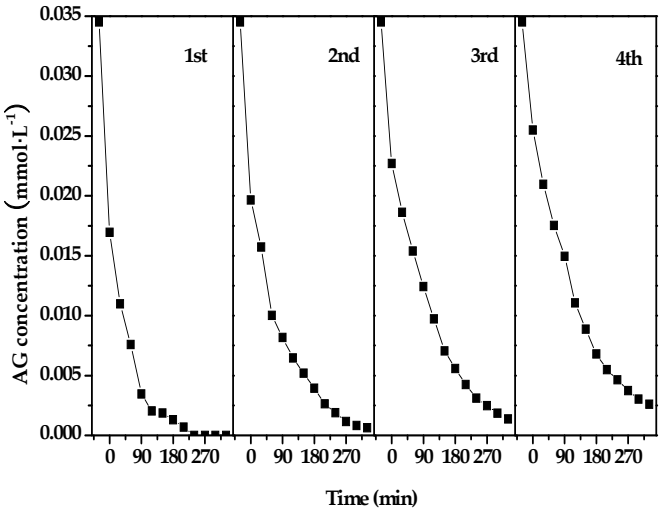

Figure 16. Repeated photocatalytic degradation tests of AG with 10% PANI-modified $BiYTi_2O_7$.

3.3. Photocatalytic Degradation Mechanism

Schematic representation of the mechanism of photocatalytic degradation AG with PANI-modified $BiYTi_2O_7$ is shown in Figure 17. PANI absorbed visible light to induce π–π* transition and transferred the excited-state electrons to the π*-orbital [70]. The delocalized π–π conjugated structures have been proven to induce a rapid photo-induced charge separation and to decrease the charge recombination rate in electron-transfer processes [83–85]. The conductive band of $BiYTi_2O_7$ and π*-orbital of PANI matched well in energy level and had chemical bond interaction [83], which could cause synergistic effect. Subsequently, based on the synergic effect, the excited-state electrons could readily inject into the conductive band of $BiYTi_2O_7$ and transfer to the surface to react with water and oxygen to yield ·OH radical and $\cdot O_2^-$ radical, which would oxidize the organic pollutants. In addition, the energy level of the highest occupied molecular orbital (HOMO) in PANI was between the conductive band and valence band of $BiYTi_2O_7$, therefore, these bands tended to combine to produce synergetic effect [70]. When different PANI-modified $BiYTi_2O_7$ photocatalysts absorbed visible light to generate electron–hole pairs, the holes in valence band of $BiYTi_2O_7$ could transfer to HOMO of PANI directly in virtue of a good match between the valence band of $BiYTi_2O_7$ and the HOMO of PANI. Since PANI was a good material for transporting holes, the photogenerated holes could emigrate to the photocatalysts surface easily and oxidize the adsorbed AG directly. Consequently, a rapid photogenerated charge separation and relatively slow charge recombination was achieved, which could dramatically enhance the photocatalytic activity of different PANI-modified $BiYTi_2O_7$ photocatalysts [73,86].

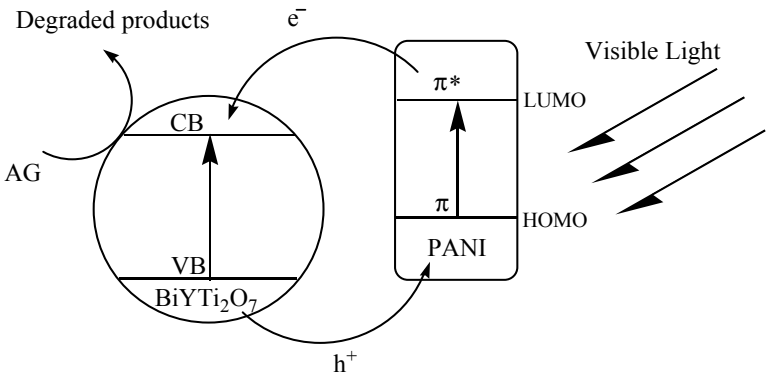

Figure 17. Schematic representation of the mechanism of photocatalytic degradation with PANI-modified $BiYTi_2O_7$.

Figure 18 shows the influence of H_2O_2 dosage (added at −30 min) on the degradation efficiency of AG (50 mL 20 mg·L^{-1}) with $BiYTi_2O_7$ (4.4 g·L^{-1}). Since reactive ·OH radical was easily generated by the breakdown of H_2O_2, the presence of H_2O_2 in the reaction mixture would take great effect on the photocatalytic process in the visible light system. The increase of H_2O_2 concentration resulted in a faster degradation of AG. It was owing to photolysis of H_2O_2 to produce ·OH radical and H_2O_2 suitable for trapping electrons by preventing the recombination of e^- and h^+ pairs [87,88]. Therefore, these phenomena increased the chance of the formation of ·OH radical and $\cdot O_2^-$ radical on the surface of the photocatalyst. The photodegradation rate of AG had been found to be much higher in the presence of H_2O_2 compared to that without H_2O_2. It was noted that above 90% photodegradation was achieved with 330 min in the presence of H_2O_2 (0.02 mol·L^{-1}) instead of 37.4% degradation in the absence of H_2O_2. It has also been widely reported that the addition of small amount of H_2O_2 greatly enhances the oxidation of organic pollutants [89–92]. The decrease mechanism in the degradation of AG in the presence of H_2O_2 was shown in the Scheme 1.

$$BiYTi_2O_7 + h\nu \rightarrow h^+ + e^-$$

$$H_2O_2 + h\nu \rightarrow 2 \cdot OH$$

$$H_2O_2 + e^- \rightarrow \cdot OH + OH^-$$

$$H_2O_2 \rightarrow 2H^+ + \cdot O_2^-$$

$$H_2O_2 + \cdot O_2^- \rightarrow \cdot OH + OH^- + O_2$$

Scheme 1. Mechanism of photocatalytic activity with H_2O_2 in the AG.

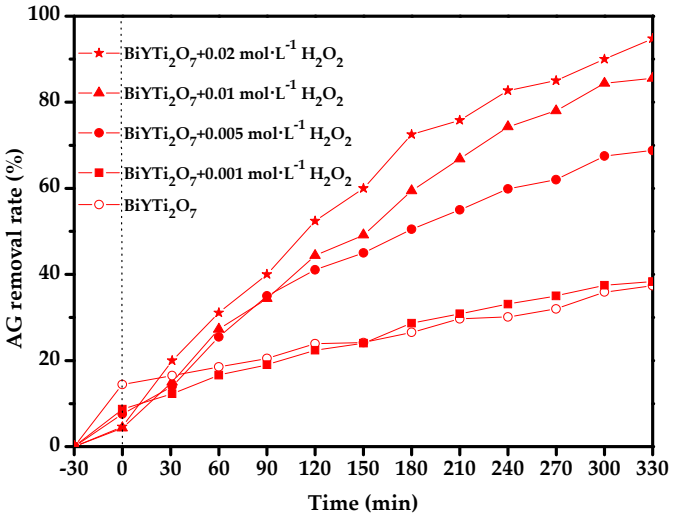

Figure 18. Influence of H_2O_2 in the degradation of AG with $BiYTi_2O_7$.

The present results indicated that different PANI-modified $BiYTi_2O_7$ photocatalysts-visible light photocatalysis system might be regarded as a potential and practical method to treat diluted colored wastewater. This system could be used for decolorization, purification and detoxification for textile, printing and dyeing industries in the long-day countries. In addition, this sort of system did not need high pressure oxygen, heating or any other chemical reagents, which could guarantee the economic sustainability. In summary, the different PANI-modified $BiYTi_2O_7$ photocatalysts–visible

light photocatalysis system might provide a valuable treatment for purifying and reusing colored aqueous effluents.

4. Conclusions

In the present work, we developed a solid-state reaction method for the preparation of $BiYTi_2O_7$ as a novel photocatalyst and a chemical oxidation polymerization method for the preparation of the novel polyaniline/$BiYTi_2O_7$ polymer composite at the first time. The as-prepared $BiYTi_2O_7$ crystallized with the pyrochlore-type structure and cubic crystal system (space group Fd3m). Meanwhile, by estimating, the value of the band gaps of $BiYTi_2O_7$ and $BiYTi_2O_7$-1% PANI were about 2.349 and 2.476 eV so that these new photocatalysts showed strong optical absorption in the visible light region. Photodegradation of AG aqueous solutions was observed under visible light irradiation in the presence of $BiYTi_2O_7$ and different PANI-modified $BiYTi_2O_7$ compared with normal photocatalyst N-doped TiO_2 in this article. Additionally, the AG removal efficiency was boosted from 3.0% for undoped $BiYTi_2O_7$ to 78.0% for the 10% PANI-modified $BiYTi_2O_7$, after only 60 min of reaction, indicating that the photocatalytic effect was enhanced with the improvement of polyaniline content in the PANI-modified $BiYTi_2O_7$ photocatalysts. The AG photodegradation with these new photocatalysts followed the first-order reaction kinetics. The synergetic effect, which was caused by the good match between the conductive band of $BiYTi_2O_7$ and the delocalized π–π conjugated structures of PANI or HOMO in PANI between the conductive band and valence band of $BiYTi_2O_7$, dramatically enhanced the photocatalytic activity of different PANI-modified $BiYTi_2O_7$ photocatalysts. Moreover, the promoter action of H_2O_2 for photocatalystic degradation by $BiYTi_2O_7$ for AG in the wastewater was discovered. In summary, different PANI-modified $BiYTi_2O_7$–Visible system might be regarded as a potential method for treating textile industry wastewater.

Acknowledgments: This work was supported by a grant from the Natural Science Foundation of Jiangsu Province (No. BK20141312), by a Project of Science and Technology Development Plan of Suzhou City of China from 2014 (No. ZXG201440), and by a grant from China-Israel Joint Research Program in Water Technology and Renewable Energy (No. 5).

Author Contributions: Jingfei Luan was involved with all aspects of the study including conceiving, designing, data interpretation and writing the manuscript. Yue Shen, Shu Wang and Ningbin Guo performed the experiments and analyzed data. Jingfei Luan and Yue Shen wrote the paper. All authors have read and approved the manuscript.

Conflicts of Interest: The authors declare no conflict of interest.

References

1. Jin, R.C.; Cao, Y.W.; Mirkin, C.A.; Kelly, K.L.; Schatz, G.C.; Zheng, J.G. Photoinduced conversion of silver nanospheres to nanoprisms. *Science* **2001**, *294*, 1901–1903. [CrossRef]
2. Lahiri, D.; Subramanian, V.; Shibata, T.; Wolf, E.E.; Bunker, B.A.; Kamat, P.V. Photoinduced transformations at semiconductor/metal interfaces: X-ray absorption studies of titania/gold films. *J. Appl. Phys.* **2003**, *93*, 2575–2582. [CrossRef]
3. Kamat, P.V. Photoinduced transformations in semiconductor-metal nanocomposite assemblies. *Pure Appl. Chem.* **2002**, *74*, 1693–1706. [CrossRef]
4. Chandrasekharan, N.; Kamat, P.V. Improving the photoelectrochemical performance of nanostructured TiO_2 films by adsorption of gold nanoparticles. *J. Phys. Chem. B* **2000**, *104*, 10851–10857.
5. Ghosh, S.; Sahu, K.; Mondal, S.K.; Sen, P.; Bhattacharyya, K. A femtosecond study of photoinduced electron transfer from dimethylaniline to coumarin dyes in a cetyltrimethylammonium bromide micelle. *J. Chem. Phys.* **2006**, *125*, 054509. [CrossRef] [PubMed]
6. Jaeger, J.B.; Pillai, E.D.; Jaeger, T.D.; Duncan, M.A. Ultraviolet and infrared photodissociation of $Si^+(C_6H_6)n$ and $Si^+(C_6H_6)n$ Ar clusters. *J. Phys. Chem. A* **2005**, *109*, 2801–2808. [CrossRef] [PubMed]
7. Kempa, T.; Farrer, R.A.; Giersig, M.; Fourkas, J.T. Photochemical synthesis and multiphoton luminescence of monodisperse silver nanocrystals. *Plasmonics* **2006**, *1*, 45–51. [CrossRef]

8. Bhatkhande, D.S.; Pangarkar, V.G.; Beenackers, A.A.C.M. Photocatalytic degradation for environmental applications—A review. *J. Chem. Technol. Biotechnol.* **2002**, *77*, 102–116. [CrossRef]
9. Breault, T.M.; Bartlett, B.M. Lowering the band gap of anatase-structured TiO_2 by coalloying with Nb and N: Electronic structure and photocatalytic degradation of methylene blue dye. *J. Phys. Chem. C* **2012**, *116*, 5986–5994. [CrossRef]
10. Kuwahara, Y.; Aoyama, J.; Miyakubo, K.; Eguchi, T.; Kamegawa, T.; Mori, K.; Yamashita, H. TiO_2 photocatalyst for degradation of organic compounds in water and air supported on highly hydrophobic FAU zeolite: Structural, sorptive, and photocatalytic studies. *J. Catal.* **2012**, *285*, 223–234. [CrossRef]
11. Da Dalt, S.; Alves, A.K.; Bergmann, C.P. Photocatalytic degradation of methyl orange dye in water solutions in the presence of MWCNT/TiO_2 composites. *Mater. Res. Bull.* **2013**, *48*, 1845–1850. [CrossRef]
12. Sinha, A.K.; Pradhan, M.; Sarkar, S.; Pal, T. Large-scale solid-state synthesis of Sn-SnO_2 nanoparticles from layered SnO by sunlight: A material for dye degradation in water by photocatalytic reaction. *Environ. Sci. Technol.* **2013**, *47*, 2339–2345. [CrossRef] [PubMed]
13. Breault, T.M.; Bartlett, B.M. Composition dependence of TiO_2:(Nb,N)-x compounds on the rate of photocatalytic methylene blue dye degradation. *J. Phys. Chem. C* **2013**, *117*, 8611–8618. [CrossRef]
14. Iyyapushpam, S.; Nishanthi, S.T.; Pathinettam Padiyan, D. Photocatalytic degradation of methyl orange using alpha-Bi_2O_3 prepared without surfactant. *J. Alloy. Compd.* **2013**, *563*, 104–107. [CrossRef]
15. Jin, S.Q.; Wang, X.; Wang, X.L.; Ju, M.G.; Shen, S.; Liang, W.Z.; Zhao, Y.; Feng, Z.C.; Playford, H.Y.; Walton, R.I. Effect of phase junction structure on the photocatalytic performance in overall water splitting: Ga_2O_3 photocatalyst as an example. *J. Phys. Chem. C* **2015**, *119*, 18221–18228. [CrossRef]
16. Srinivasu, K.; Modak, B.; Ghosh, S.K. Porous graphitic carbon nitride: A possible metal-free photocatalyst for water splitting. *J. Phys. Chem. C* **2014**, *118*, 26479–26484. [CrossRef]
17. Lee, K.M.; Lai, C.W.; Ngai, K.S.; Juan, J.C. Recent developments of zinc oxide based photocatalyst in water treatment technology: A review. *Water Res.* **2016**, *88*, 428–448. [CrossRef] [PubMed]
18. Liyanage, A.D.; Perera, S.D.; Tan, K.; Chabal, Y.; Balkus, K.J. Synthesis, characterization, and photocatalytic activity of Y-doped CeO_2 nanorods. *ACS Catal.* **2014**, *4*, 577–584. [CrossRef]
19. Yu, X.L.; Shavel, A.; An, X.Q.; Luo, Z.S.; Ibanez, M.; Cabot, A. Cu_2ZnSnS_4-Pt and Cu_2ZnSnS_4-Au heterostructured nanoparticles for photocatalytic water splitting and pollutant degradation. *J. Am. Chem. Soc.* **2014**, *136*, 9236–9239. [CrossRef] [PubMed]
20. Zhou, X.M.; Xu, Q.L.; Lei, W.Y.; Zhang, T.T.; Qi, X.Y.; Liu, G.; Deng, K.; Yu, J.G. Origin of tunable photocatalytic selectivity of well-defined alpha-Fe_2O_3 nanocrystals. *Small* **2014**, *10*, 674–679. [CrossRef] [PubMed]
21. Wang, L.L.; Wang, J.F.; Zhang, Y.; Ding, Z.T.; Cao, Q.E. Investigation on the determination of proteins by spectrophotometry with azocarmine G. *J. Yunnan Univ. Nat. Sci.* **2008**, *30*, 83–86.
22. Chen, Z.G.; Ren, F.L.; Si, S.H.; Liao, X.H.; Ding, W.F.; Liu, J.B. Sensitive determination of DNA based on resonance light scattering enhancement of Azocarmine G and CTAB. *J. Cent. South Univ. Technol.* **2005**, *12*, 688–692. [CrossRef]
23. Murakami, T.; Mahmut, N.; Hitomi, S.; Ohtsuka, A. Dark and light neurons in the human brain, with special reference to their reactions to Golgi's silver nitrate, luxol fast blue MBS and azocarmine G. *Arch. Histol. Cytol.* **1997**, *60*, 265–274. [CrossRef] [PubMed]
24. Low, G.K.C.; Mcevoy, S.R.; Matthews, R.W. Formation of nitrate and ammonium-ions in titanium-dioxideI mediated photocatalytic degradation of organic-compounds containing nitrogen-atoms. *Environ. Sci. Technol.* **1991**, *25*, 460–467. [CrossRef]
25. Matos, J.; Laine, J.; Herrmann, J.M. Effect of the type of activated carbons on the photocatalytic degradation of aqueous organic pollutants by UV-irradiated titania. *J. Catal.* **2001**, *200*, 10–20. [CrossRef]
26. Khodja, A.A.; Lavedrine, B.; Richard, C.; Sehili, T. Photocatalytic degradation of metoxuron in aqueous suspensions of TiO_2 analytical and kinetic studies. *Int. J. Photoenergy* **2002**, *4*, 147–151. [CrossRef]
27. Zhao, W.; Ma, W.H.; Chen, C.C.; Zhao, J.C.; Shuai, Z.G. Efficient degradation of toxic organic pollutants with Ni_2O_3/TiO_2-*x*B*x* under visible irradiation. *J. Am. Chem. Soc.* **2004**, *126*, 4782–4783. [CrossRef] [PubMed]
28. Murashkina, A.A.; Murzin, P.D.; Rudakova, A.V.; Ryabchuk, V.K.; Emeline, A.V.; Bahnemann, D.W. Influence of the dopant concentration on the photocatalytic activity: Al-doped TiO_2. *J. Phys. Chem. C* **2015**, *119*, 24695–24703. [CrossRef]

29. Lu, F.; Cai, W.P.; Zhang, Y.G. ZnO Hierarchical micro/nanoarchitectures: Solvothermal synthesis and structurally enhanced photocatalytic performance. *Adv. Funct. Mater.* **2008**, *18*, 1047–1056. [CrossRef]
30. Kitano, M.; Takeuchi, M.; Matsuoka, M.; Thomas, J.M.; Anpo, M. Preparation of visible light-responsive TiO_2 thin film photocatalysts by an RF magnetron sputtering deposition method and their photocatalytic reactivity. *Chem. Lett.* **2005**, *34*, 616–617. [CrossRef]
31. Chatterjee, D.; Dasgupta, S. Visible light induced photocatalytic degradation of organic pollutants. *J. Photochem. Photobiol. C.* **2005**, *6*, 186–205. [CrossRef]
32. Zhao, J.C.; Chen, C.C.; Ma, W.H. Photocatalytic degradation of organic pollutants under visible light irradiation. *Top. Catal.* **2005**, *35*, 269–278. [CrossRef]
33. Zou, Z.G.; Ye, J.H.; Sayama, K.; Arakawa, H. Direct splitting of water under visible light irradiation with an oxide semiconductor photocatalyst. *Nature* **2001**, *414*, 625–627. [CrossRef] [PubMed]
34. Sivalingam, G.; Madras, G. Photocatalytic degradation of poly(bisphenol-A-carbonate) in solution over combustion-synthesized TiO_2: Mechanism and kinetics. *Appl. Catal. A.* **2004**, *269*, 81–90. [CrossRef]
35. Maeda, K.; Terashima, H.; Kase, K.; Higashi, M.; Tabata, M.; Domen, K. Surface modification of TaON with monoclinic ZrO_2 to produce a composite photocatalyst with enhanced hydrogen evolution activity under visible light. *Bull. Chem. Soc. Jpn.* **2008**, *81*, 927–937. [CrossRef]
36. Shi, H.X.; Chen, J.Y.; Li, G.Y.; Nie, X.; Zhao, H.J.; Wong, P.K.; An, T.C. Synthesis and characterization of novel plasmonic Ag/AgX-CNTs (X = Cl, Br, I) nanocomposite photocatalysts and synergetic degradation of organic pollutant under visible light. *ACS Appl. Mater. Interfaces* **2013**, *5*, 6959–6967. [CrossRef] [PubMed]
37. Ge, L.; Han, C.C.; Liu, J. In situ synthesis and enhanced visible Light photocatalytic activities of novel PANI-g-C_3N_4 composite photocatalysts. *J. Mater. Chem.* **2012**, *22*, 11843–11850. [CrossRef]
38. He, G.H.; Liang, C.J.; Ou, Y.D.; Liu, D.N.; Fang, Y.P.; Xu, Y.H. Preparation of novel Sb_2O_3/WO_3 photocatalysts and their activities under visible light irradiation. *Mater. Res. Bull.* **2013**, *48*, 2244–2249. [CrossRef]
39. Wang, J.X.; Ruan, H.; Li, W.J.; Li, D.Z.; Hu, Y.; Chen, J.; Shao, Y.; Zheng, Y. Highly efficient oxidation of gaseous benzene on novel Ag_3VO_4/TiO_2 nanocomposite photocatalysts under visible and simulated solar light irradiation. *J. Phys. Chem. C* **2012**, *116*, 13935–13943. [CrossRef]
40. Kameyama, T.; Takahashi, T.; Machida, T.; Kamiya, Y.; Yamamoto, T.; Kuwabata, S.; Torimoto, T. Controlling the electronic energy structure of ZnS-$AgInS_2$ solid solution nanocrystals for photoluminescence and photocatalytic hydrogen evolution. *J. Phys. Chem. C* **2015**, *119*, 24740–24749. [CrossRef]
41. Teng, F.; Liu, Z.L.; Zhang, A.; Li, M. Photocatalytic performances of Ag_3PO_4 polypods for degradation of dye pollutant under natural indoor weak light irradiation. *Environ. Sci. Technol.* **2015**, *49*, 9489–9494. [CrossRef] [PubMed]
42. Han, S.C.; Hu, L.F.; Liang, Z.Q.; Wageh, S.; Al-Ghamdi, A.A.; Chen, Y.S.; Fang, X.S. One-step hydrothermal synthesis of 2D hexagonal nanoplates of alpha-Fe_2O_3/graphene composites with enhanced photocatalytic activity. *Adv. Funct. Mater.* **2014**, *24*, 5719–5727. [CrossRef]
43. Luan, J.F.; Li, Y.Y. Photocatalytic water splitting for hydrogen production with Gd_2MSbO_7 (M = Fe, In, Y) photocatalysts under visible light irradiation. *Materials* **2015**, *8*, 16–30. [CrossRef]
44. Liu, W.; Ji, M.S.; Chen, S.F. Preparation, characterization and activity evaluation of $Ag_2Mo_4O_{13}$ photocatalyst. *J. Hazard. Mater.* **2011**, *186*, 2001–2008. [CrossRef] [PubMed]
45. Zhao, J.; Dong, W.W.; Wu, Y.P.; Wang, Y.N.; Wang, C.; Li, D.S.; Zhang, Q.C. Two (3,6)-connected porous metal-organic frameworks based on linear trinuclear [Co-3(COO)(6)] and paddlewheel dinuclear [Cu-2(COO)(4)] SBUs: Gas adsorption, photocatalytic behaviour, and magnetic properties. *J. Mater. Chem. A* **2015**, *3*, 6962–6969. [CrossRef]
46. Gao, J.K.; Miao, J.W.; Li, P.Z.; Teng, W.Y.; Yang, L.; Zhao, Y.L.; Liu, B.; Zhang, Q.C. A p-type Ti(IV)-based metal-organic framework with visible-light photo-response. *Chem. Commun.* **2014**, *50*, 3786–3788. [CrossRef] [PubMed]
47. Gao, J.K.; Cao, S.W.; Tay, Q.L.; Liu, Y.; Yu, L.M.; Ye, K.Q.; Mun, P.C.S.; Li, Y.X.; Rakesh, G.; Loo, S.C.J.; et al. Molecule-based water-oxidation catalysts (WOCs): Cluster-size-dependent dye-sensitized polyoxometalates for visible-light-driven O_2 evolution. *Sci. Rep.* **2013**, *3*, 1853. [CrossRef] [PubMed]
48. Luan, J.F.; Ma, K.; Pan, B.C.; Li, Y.M.; Wu, X.S.; Zou, Z.G. Synthesis and catalytic activity of new Gd_2BiSbO_7 and Gd_2YSbO_7 nanocatalysts. *J. Mol. Catal. A Chem.* **2010**, *321*, 1–9. [CrossRef]
49. Luan, J.F.; Ma, K.; Li, Y.M.; Zou, Z.G. Photophysical and photocatalytic properties of novel Y_2GaSbO_7 and Y_2YbSbO_7 photocatalysts under visible light irradiation. *J. Mater. Sci.* **2011**, *46*, 813–823. [CrossRef]

50. Luan, J.F.; Li, M.; Ma, K.; Li, Y.M.; Zou, Z.G. Photocatalytic activity of novel Y_2InSbO_7 and Y_2GdSbO_7 nanocatalysts for degradation of environmental pollutant rhodamine B under visible light irradiation. *Chem. Eng. J.* **2011**, *167*, 162–171. [CrossRef]
51. Luan, J.F.; Cai, H.L.; Zheng, S.R.; Hao, X.P.; Luan, G.Y.; Wu, X.S.; Zou, Z.G. Structural and photocatalytic properties of novel Bi_2GaVO_7. *Mater. Chem. Phys.* **2007**, *104*, 119–124. [CrossRef]
52. Luan, J.F.; Cai, H.L.; Hao, X.P.; Zhang, J.B.; Luan, G.Y.; Wu, X.S.; Zou, Z.G. Structural characterization and photocatalytic properties of novel Bi_2FeVO_7. *Res. Chem. Intermed.* **2007**, *33*, 487–500. [CrossRef]
53. Barka, N.; Assabbane, A.; Nounah, A.; Ichou, Y.A. Photocatalytic degradation of indigo carmine in aqueous solution by TiO_2-coated non-woven fibres. *J. Hazard. Mater.* **2008**, *152*, 1054–1059. [CrossRef] [PubMed]
54. Chen, X.; Mao, S.S. Titanium dioxide nanomaterials: Synthesis, properties, modifications, and applications. *Chem. Rev.* **2007**, *107*, 2891–2959. [CrossRef] [PubMed]
55. Cheng, H.; Huang, B.; Dai, Y.; Qin, X.; Zhang, X.; Wang, Z.; Jiang, M. Visible-light photocatalytic activity of the metastable $Bi_{20}TiO_{32}$ synthesized by a high-temperature quenching method. *J. Solid State Chem.* **2009**, *182*, 2274–2278. [CrossRef]
56. Guillard, C.; Disdier, J.; Monnet, C.; Dussaud, J.; Malato, S.; Blanco, J.; Maldonado, M.I.; Herrmann, J.M. Solar efficiency of a new deposited titania photocatalyst: Chlorophenol, pesticide and dye removal applications. *Appl. Catal. B* **2003**, *46*, 319–332. [CrossRef]
57. Dong, F.; Li, Q.Y.; Sun, Y.J.; Ho, W.K. Noble metal-like behavior of plasmonic Bi particles as a cocatalyst deposited on $(BiO)_2CO_3$ microspheres for efficient visible light photocatalysis. *ACS Catal.* **2014**, *4*, 4341–4350. [CrossRef]
58. Yang, D.R.; Feng, J.; Jiang, L.L.; Wu, X.L.; Sheng, L.Z.; Jiang, Y.T.; Wei, T.; Fan, Z.J. Photocatalyst interface engineering: Spatially confined growth of $ZnFe_2O_4$ within graphene networks as excellent visible-light-driven photocatalysts. *Adv. Funct. Mater.* **2015**, *25*, 7080–7087. [CrossRef]
59. Li, G.Y.; Nie, X.; Chen, J.Y.; Jiang, Q.; An, T.C.; Wong, P.K.; Zhang, H.M.; Zhao, H.J.; Yamashita, H. Enhanced visible-light-driven photocatalytic inactivation of *Escherichia coli* using g-C_3N_4/TiO_2 hybrid photocatalyst synthesized using a hydrothermal-calcination approach. *Water Res.* **2015**, *86*, 17–24. [CrossRef] [PubMed]
60. Zhang, G.; Hu, Z.Y.; Sun, M.; Liu, Y.; Liu, L.M.; Liu, H.J.; Huang, C.P.; Qu, J.H.; Li, J.H. Formation of Bi_2WO_6 bipyramids with vacancy pairs for enhanced solar-driven photoactivity. *Adv. Funct. Mater.* **2015**, *25*, 3726–3734. [CrossRef]
61. Li, N.; Li, Y.M.; Li, W.J.; Ji, S.D.; Jin, P. One-step hydrothermal synthesis of TiO_2@MoO_3 core-shell nanomaterial: Microstructure, growth mechanism, and improved photochromic property. *J. Phys. Chem. C* **2016**, *120*, 3341–3349. [CrossRef]
62. Gnayem, H.; Sasson, Y. Nanostructured 3D sunflower-like bismuth doped $BiOCl_xBr_{1-x}$ solid solutions with enhanced visible light photocatalytic activity as a remarkably efficient technology for water Purification. *J. Phys. Chem. C* **2015**, *119*, 19201–19209. [CrossRef]
63. Li, H.L.; Yu, K.; Lei, X.; Guo, B.J.; Fu, H.; Zhu, Z.Q. Hydrothermal synthesis of novel MoS_2/$BiVO_4$ hetero-nanoflowers with enhanced photocatalytic activity and a mechanism investigation. *J. Phys. Chem. C* **2015**, *119*, 22681–22689. [CrossRef]
64. Grigioni, I.; Stamplecoskie, K.G.; Selli, E.; Kamat, P.V. Dynamics of photogenerated charge carriers in WO_3/$BiVO_4$ heterojunction photoanodes. *J.Phys. Chem. C* **2015**, *119*, 20792–20800. [CrossRef]
65. Luan, J.F.; Wang, S.; Ma, K.; Li, Y.M.; Pan, B.C. Structural property and catalytic activity of new In_2YbSbO_7 and Gd_2YbSbO_7 nanocatalysts under visible light irradiation. *J. Phys. Chem. C* **2010**, *114*, 9398–9407. [CrossRef]
66. El Jaouhari, A.; Laabd, M.; Aouzal, Z.; Bouabdallaoui, M.; Bazzaoui, E.A.; Albourine, A.; Martins, J.I.; Wang, R.; Bazzaoui, M. Effect of electrolytic conditions on PANi electrosynthesis on stainless steel: A new application to polycarboxy-benzoic acids removal from industrial effluents. *Prog. Org. Coat.* **2016**, *101*, 233–239. [CrossRef]
67. Negi, Y.S.; Adhyapak, P.V. Development in polyaniline conducting polymers. *J. Macromol. Sci. Polym. Rev.* **2002**, *42*, 35–53. [CrossRef]
68. Xie, J.; Zhao, C.E.; Lin, Z.Q.; Gu, P.Y.; Zhang, Q.C. Nanostructured conjugated polymers for energy-related applications beyond solar cells. *Chem. Asian J.* **2016**, *11*, 1489–1511. [CrossRef] [PubMed]

69. Pandiselvi, K.; Fang, H.F.; Huang, X.B.; Wang, J.Y.; Xu, X.C.; Li, T. Constructing a novel carbon nitride/polyaniline/ZnO ternary heterostructure with enhanced photocatalytic performance using exfoliated carbon nitride nanosheets as supports. *J. Hazard. Mater.* **2016**, *314*, 67–77. [CrossRef] [PubMed]
70. Shang, M.; Wang, W.Z.; Sun, S.M.; Ren, J.; Zhou, L.; Zhang, L. Efficient visible light-induced photocatalytic degradation of contaminant by spindle-like PANI/$BiVO_4$. *J. Phys. Chem. C* **2009**, *113*, 20228–20233. [CrossRef]
71. Hidalgo, D.; Bocchini, S.; Fontana, M.; Saracco, G.; Hernandez, S. Green and low-cost synthesis of PANI-TiO_2 nanocomposite mesoporous films for photoelectrochemical water splitting. *RSC Adv.* **2015**, *5*, 49429–49438. [CrossRef]
72. Zou, Z.G.; Ye, J.H.; Arakawa, H. Compositional dependence of crystallization in the glass-ceramics system Bi_2O_3-In_2O_3-MnO_2-B_2O_3. *J. Mater. Sci. Lett.* **2000**, *19*, 1909–1911. [CrossRef]
73. Zhang, H.; Zong, R.L.; Zhao, J.C.; Zhu, Y.F. Dramatic visible photocatalytic degradation performances due to synergetic effect of TiO_2 with PANI. *Environ. Sci. Technol.* **2008**, *42*, 3803–3807. [CrossRef] [PubMed]
74. Chen, L.X.; Rajh, T.; Wang, Z.Y.; Thurnauer, M.C. XAFS studies of surface structures of TiO_2 nanoparticles and photocatalytic reduction of metal ions. *J. Phys. Chem. B* **1997**, *101*, 10688–10697. [CrossRef]
75. Chen, W.F.; Koshy, P.; Huang, Y.; Adabifiroozjaei, E.; Yao, Y.; Sorrell, C.C. Effects of precipitation, liquid formation, and intervalence charge transfer on the properties andphotocatalytic performance of cobalt- or vanadium-doped TiO_2 thin films. *J. Hydrogen Energy* **2016**, *41*, 19025–19056. [CrossRef]
76. Liao, Y.H.B.; Wang, J.X.; Lin, J.S.; Chung, W.H.; Lin, W.Y.; Chen, C.C. Synthesis, photocatalytic activities and degradation mechanism of Bi_2WO_6 toward crystal violet dye. *Catal. Today* **2011**, *174*, 148–159. [CrossRef]
77. Tauc, J.; Grigorov, R.; Vancu, A. Optical properties and electronic structure of amorphous germanium. *Phys. Status Solidi* **1966**, *15*, 627–637. [CrossRef]
78. Butler, M.A. Photoelectrolysis with $YFeO_3$ electrodes. *J. Appl. Phys.* **1977**, *48*, 1914–1920. [CrossRef]
79. Oshikiri, M.; Boero, M.; Ye, J.H.; Zou, Z.G.; Kido, G. Electronic structures of promising photocatalysts $InMO_4$ (M=V, Nb, Ta) and $BiVO_4$ for water decomposition in the visible wavelength region. *J. Chem. Phys.* **2002**, *117*, 7313–7318. [CrossRef]
80. Liu, G.M.; Wu, T.X.; Zhao, J.C.; Hidaka, H.; Serpone, N. Photoassisted degradation of dye pollutants. 8. Irreversible degradation of alizarin red under visible light radiation in air-equilibrated aqueous TiO_2 dispersions. *Environ. Sci. Technol.* **1999**, *33*, 2081–2087. [CrossRef]
81. Reddy, V.R.; Hwang, D.W.; Lee, J.S. Effect of Zr substitution for Ti in $KLaTiO_4$ for photocatalytic water splitting. *Catal. Lett.* **2003**, *90*, 39–43. [CrossRef]
82. Sun, H.; Qiu, G.H.; Wang, Y.; Feng, X.H.; Yin, H.; Liu, F. Effects of Co and Ni co-doping on the physicochemical properties of cryptomelane and its enhanced performance on photocatalytic degradation of phenol. *Mater. Chem. Phys.* **2014**, *148*, 783–789. [CrossRef]
83. Liu, L.; Ding, L.; Liu, Y.G.; An, W.J.; Lin, S.L.; Liang, Y.H.; Cui, W.Q. A stable Ag_3PO_4@PANI core@shell hybrid: Enrichment photocatalytic degradation with pi-pi conjugation. *Appl. Catal. B* **2017**, *210*, 92–104. [CrossRef]
84. Williams, G.; Seger, B.; Kamat, P.V. TiO_2-graphene nanocomposites. UV-assisted photocatalytic reduction of graphene oxide. *ACS Nano* **2008**, *2*, 1487–1491. [CrossRef] [PubMed]
85. Zhu, S.B.; Xu, T.G.; Fu, H.B.; Zhao, J.C.; Zhu, Y.F. Synergetic effect of Bi_2WO_6 photocatalyst with C-60 and enhanced photoactivity under visible irradiation. *Environ. Sci. Technol.* **2007**, *41*, 6234–6239. [CrossRef] [PubMed]
86. Ameen, S.; Akhtar, M.S.; Kim, Y.S.; Yang, O.B.; Shin, H.S. An effective nanocomposite of polyaniline and ZnO: Preparation, characterizations, and its photocatalytic activity. *Colloid Polym. Sci.* **2011**, *289*, 415–421. [CrossRef]
87. Hou, J.G.; Cao, R.; Jiao, S.Q.; Zhu, H.M.; Kumar, R.V. PANI/$Bi_{12}TiO_{20}$ complex architectures: Controllable synthesis and enhanced visible-light photocatalytic activities. *Appl. Catal. B* **2011**, *104*, 399–406. [CrossRef]
88. Chen, H.H.; Xiong, X.Q.; Hao, L.L.; Zhang, X.; Xu, Y.M. Improved visible light photocatalytic activity of WO_3 through $CuWO_4$ for phenol degradation. *Appl. Surf. Sci.* **2016**, *389*, 491–495. [CrossRef]
89. Neppolian, B.; Kanel, S.R.; Choi, H.C.; Shankar, M.V.; Arabindoo, B.; Murugesan, V. Photocatalytic degradation of reactive yellow 17 dye in aqueous solution in the presence of TiO_2 with cement binder. *Int. J. Photoenergy* **2003**, *5*, 45–49. [CrossRef]
90. Muruganandham, M.; Swaminathan, M. Solar photocatalytic degradation of a reactive azo dye in TiO_2-suspension. *Sol. Energy Mater. Sol. Cells* **2004**, *81*, 439–457. [CrossRef]

91. Wang, G.L.; Xu, X.F.; Wu, X.M.; Cao, G.X.; Dong, Y.M.; Li, Z.J. Visible-light-stimulated enzymelike activity of graphene oxide and its application for facile glucose sensing. *J. Phys. Chem. C* **2014**, *118*, 28109–28117. [CrossRef]
92. Ng, T.W.; Zhang, L.S.; Liu, J.S.; Huang, G.C.; Wang, W.; Wong, P.K. Visible-light-driven photocatalytic inactivation of escherichia coli by magnetic Fe_2O_3-AgBr. *Water Res.* **2016**, *90*, 111–118. [CrossRef] [PubMed]